

Załącznik nr 4

Autoreferat w języku angielskim

Summary of professional accomplishments

## 1 Name and surname

---

Agnieszka Słowikowska

## 2 Degrees with name, place, and year, as well as with a title of a PhD thesis

---

- Doctor of Philosophy in physical sciences in the field of astronomy given by the resolution of the Council of the Nicolaus Copernicus Astronomical Center of the Polish Academy of Science, Warsaw, October 26th, 2006, thesis title: „Pulsar Characteristics Across the Energy Spectrum”,
- Master of Science degree awarded by the Faculty of Physics, Astronomy and Informatics of the Nicolaus Copernicus University in Toruń, June 12th, 2001.

## 3 Information on employment

---

- from October 1st, 2017 until now: assistant professor in the Department of Astronomy and Astrophysics of the Centre for Astronomy of the Nicolaus Copernicus University in Toruń,
- from October 1st, 2009 to September 30th, 2017: assistant professor in the Faculty of Physics and Astrophysics of the University of Zielona Góra,
- from January 1st, 2007 until August 31st, 2009: *post-doc* at Foundation for Research and Technology - Hellas, Heraklion, Greece,
- from November 1st, 2006 to January 2nd, 2009: assistant professor at the Nicolaus Copernicus Astronomical Center of the Polish Academy of Science, Warsaw.

## 4 The scientific achievement, in accordance with art.16 paragraph 2 of the Act of March 14th, 2003, concerning the scientific degrees and titles (Dz. U. item no. 882, 2016, with amendments in Dz. U. item no. 1311, 2016)

---

a) Title of the scientific achievement

**High time resolution photopolarimetric studies of white dwarfs and neutron stars in the radio and optical domain**

b) List of publications constituting the scientific achievement (author/authors, title, date, journal/publisher name)

**H1 Słowikowska, Agnieszka;** Stappers, Benjamin W.; Harding, Alice K.; O'Dell, Stephen L.; Elsner, Ronald F.; van der Horst, Alexander J.; Weisskopf, Martin C.; "High-time-resolution Measurements of the Polarization of the Crab Pulsar at 1.38 GHz"; 2015, The Astrophysical Journal, Volume 799, Issue 1, article id. 70, 12 pp., (Słowikowska et al., 2015);

**H2 Słowikowska, Agnieszka;** Krzeszowski, Krzysztof; Żejmo, Michał; Blinov, Dmitry; Reig, Pablo; "Optical linear polarization of helium-rich white dwarfs sample with the RoboPOL polarimeter"; 2018; Monthly Notices of the Royal Astronomical Society, Volume 479, Issue 4, p.5312-5324; (Słowikowska et al., 2018);

**H3 Żejmo, Michał; Słowikowska, Agnieszka;** Krzeszowski, Krzysztof; Reig, Pablo; Blinov, Dmitry; "Optical linear polarization of 74 white dwarfs with the RoboPOL polarimeter"; 2017; Monthly Notices of the Royal Astronomical Society, Volume 464, Issue 2, p.1294-1305; (Żejmo et al., 2017);

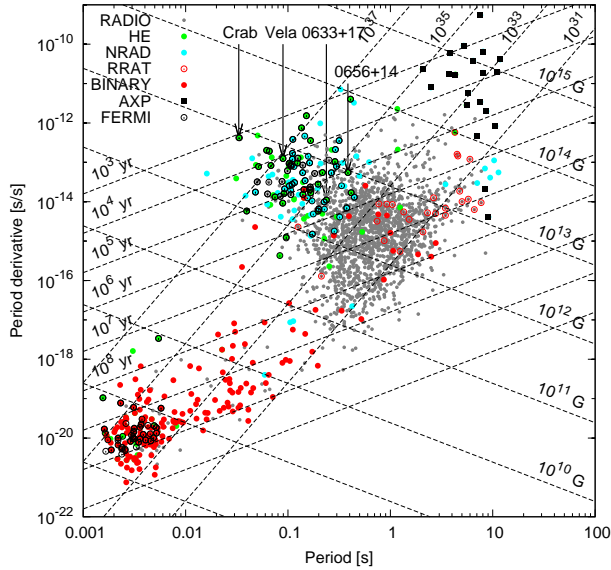


Fig. 1.  $P-\dot{P}$  plot based on the ATNF and the FERMI pulsar catalogue. Small grey filled circles denote radio pulsars, green filled circles denote spin-powered pulsars with pulsed emission from radio to infrared or higher frequencies (HE), blue filled circles denote spin-powered pulsars with pulsed emission only at infrared or higher frequencies (NRAD), red open circles denote pulsars with intermittently pulsed radio emission (RRAT), red filled circles denote pulsars in binary systems (BINARY), black filled squares denote Anomalous X-ray Pulsars or Soft Gamma-ray Repeaters with detected pulsations (AXP) and black open circles denote pulsars detected with FERMI Satellite. Dashed lines denote age (yr), magnetic field (G) and spindown energy loss rate (erg/s). Four pulsars, i.e. Crab, Vela, Geminga (0633+17) and 0656+14 are marked with arrows. All four are relatively young with high magnetic field strength.

**H4** Słowikowska, Agnieszka; Krzeszowski, Krzysztof; Żejmo, Michał; Reig, Pablo; Steele, Iain; "Calibration of the Liverpool Telescope RINGO3 polarimeter"; 2016; Monthly Notices of the Royal Astronomical Society, Volume 458, Issue 1, p.759-771; (Słowikowska et al., 2016);

**H5** Nasiroglu, Ilham; Słowikowska, Agnieszka; Kanbach, Gottfried; Haberl, Frank; "Very fast photometric and X-ray observations of the intermediate polar V2069 Cygni (RX J2123.7+4217)"; 2012; Monthly Notices of the Royal Astronomical Society, Volume 420, Issue 4, pp. 3350-3359; (Nasiroglu et al., 2012);

**H6** Reig, Pablo; Słowikowska, Agnieszka; Zezas, Andreas; Blay, Pere; "Correlated optical/X-ray variability in the high-mass X-ray binary SAX J2103.5+4545"; 2010; Monthly Notices of the Royal Astronomical Society, Volume 401, Issue 1, pp. 55-66; (Reig et al., 2010);

**H7** Stefanescu, Alex; Kanbach, Gottfried; Słowikowska, Agnieszka; Greiner, Jochen; McBreten, Sheila; Sala, Gloria; "Very fast optical flaring from a possible new Galactic magnetar"; 2008; Nature, Volume 455, Issue 7212, pp. 503-505; (Stefanescu et al., 2008).

- c) Description of the scientific objectives and the research results presented in the scientific achievement, together with the discussion of their possible applications

## 4.1 Introduction

The analysis of the electromagnetic radiation from a celestial source allows one to obtain a wealth of fundamental information about its main characteristics, e.g. the physical processes that produced the radiation, the properties of the source environment, and the mechanisms influencing the radiation propagation in the interstellar medium (ISM). In particular, photons carry information on their energy, arrival direction, on the orientation of the electric and magnetic field vectors, and, not ultimately, on the geometry of the space-time in which they propagate. This information can be decoded using a variety of techniques and deploying different instrument set-ups. Polarimetry is an almost as traditional technique as photometry and spectroscopy in astronomical observations. It has been crucial to investigate the effects of light propagation in a vacuum or the ISM and, together with spectroscopy, obtain information on the physical processes that produce electromagnetic radiation and their dependence on, e.g. the magnetic field strength and geometry at the source.

While spectroscopy, photometry, and timing are techniques applied at all wavelengths, polarimetry has been so far used mainly in the radio and in the optical domains. As X and gamma-ray polarimetry establish these days, optical polarimetry has been pivotal in studying a variety of incoherent emission mechanisms, synchrotron and curvature radiation, from several types of sources: compact objects (neutron stars, white dwarfs, black holes), interacting binaries, active galactic nuclei (AGN), etc. Some of these studies investigate the properties of the extreme magnetic fields around neutron stars and map the magnetic and electric field in diffuse emission environments, such as supernova remnants (SNR) or pulsar-wind nebulae (PWN).

Neutron stars, and especially those observed as pulsars, are one of the best sources of polarized radiation across the electromagnetic spectrum, especially in gamma regime, where the polarization degree is estimated to be as high as 100%. Today we know of more than 2659 radio pulsars, according to the *Australia Telescope National Facility Pulsar Catalogue* (Manchester et al., 2005), out of which around 10% is observed in X-ray (mainly in binary systems). However, only a few of them are detected in the optical regime. Different types of pulsars are shown in the P- $\dot{P}$  diagram (rotational period - rotational period first derivative diagram), Fig. 1.

High time-resolved observations of pulsars provide important astrophysical information about their magnetic field configuration, magnetosphere structure, and the plasma energy distribution therein. Despite over fifty years of observation, the emission mechanism of rotation-powered pulsars (RPP) is still a matter of considerable debate. A broad consensus does exist - the luminosity is rotation powered, the pulsed radio signal is coherent in origin, the optical emission is synchrotron radiation while in the  $\gamma$ -ray region it becomes curvature radiation and inverse Compton for the highest energy photons. What is not agreed on is the mechanism that accelerates the electrons to the energy required for synchrotron and curvature radiation and where this acceleration takes place. Optical emission from pulsars is generally agreed to come from incoherent synchrotron radiation which is highly polarised with its linear polarization vector oriented parallel to the radius of curvature of the magnetic field at the emission region. The time-resolved observation of the changes in the alignment of the polarization vector within a rotational period of the neutron star, therefore, gives direct information on the orientation of the magnetic field lines at the respective emitting region. While in the case of young pulsars pure synchrotron radiation leads to a relatively high optical emission efficiency and power-law spectrum (e.g. Hill et al. 1997), the spectral shapes of older pulsars are more complex, suggesting a mixture of magnetospheric and thermal radiation at lower emission efficiencies. With increasing age and slow down, the magnetospheric component of the optical emission seems to become weaker, increasing the significance of the thermal component, which in the end dominates the optical emission of the pulsar.

Within a large sample of radio pulsars that exceeds more than 2600 objects, there are only a few known and identified optical pulsars. Within this group, only for one (i.e. the Crab pulsar, Smith et al., 1988; Słowińska et al., 2009), the fully phase-resolved optical polarimetry is known. To understand deeper the radiation mechanism of pulsars we need to investigate not only their light curves and spectral characteristics, but also polarized part of their emission. What has been not possible to date are the phase-resolved observations of the polarization of the optical radiation from pulsars (apart from the Crab pulsar). It is a difficult and challenging task, while pulsars are not only very faint in the optical domain, but they also rotate very fast. Therefore, very sensitive and at the same time capable of performing observations with high time resolution photopolarimeter are required. These types of optical photopolarimeters are scarce instruments.

## 4.2 Radio Polarimetry of the Crab pulsar at 1.38 GHz [H1]

The Crab pulsar's light curve exhibits different features at different wavelengths, but it is currently the only pulsar for which the two principal features, main pulse (MP) and interpulse (IP),

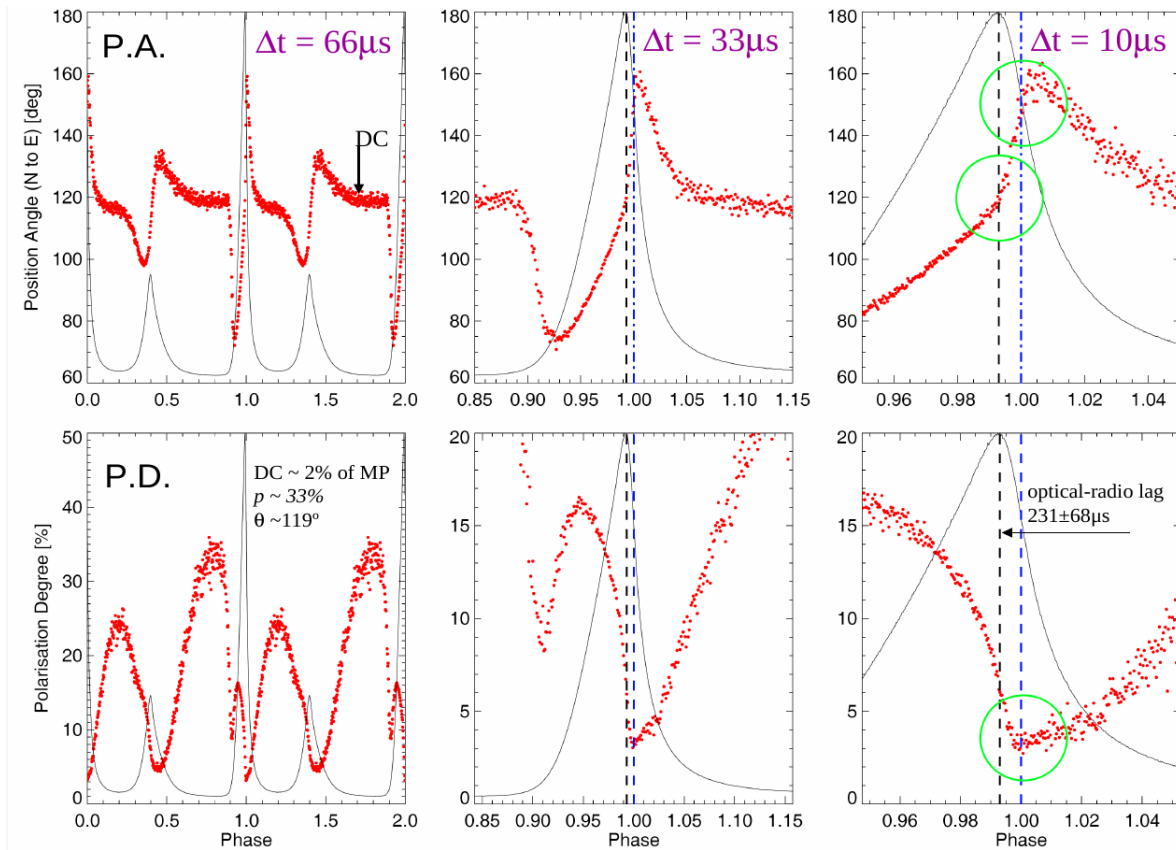


Fig. 2. *Top*: Crab pulsar observed with OPTIMA photopolarimeter position angle (PA) as a function of rotational phase, where the left (two pulses are shown for clarity), middle, and right panels center on different parts of the phase curve (Słowiowska et al., 2009). Abrupt PA changes are aligned with the main pulse in both the optical (vertical dashed black line) and the radio (vertical dashed blue line). *Bottom*: Crab pulsar polarization degree (PD) as a function of rotational phase. Optical PD minimum is correlated with the radio intensity peak (vertical dashed blue line), and not for the optical peak (vertical dashed black line).

persist over all wavelengths. They also appear at roughly the same pulse phase, from radio to  $\gamma$ -ray. However, at the radio frequencies situation changes and the Crab light curve gets up to six peaks: LFC - low frequency component, precursor, MP, IP, HFC1 - high frequency component one, and HFC2 - high frequency component two. During my research, I have performed the high time-resolved optical observations of the Crab pulsar with the OPTical TIMing Analyzer (OPTIMA<sup>1</sup>). The Crab pulsar rotates with the 34 milliseconds period. The time bin width of the optical polarization characteristics was 4  $\mu$ s and it is shown in Fig. 2 (Słowikowska et al., 2009)<sup>2</sup>. To solve the puzzle of the emission of the Crab pulsar, a multiwavelength study of its polarization across the spectrum is necessary. The review of the polarization characteristics at radio frequencies from 1.4 GHz to 8.4 GHz was performed and presented by Moffett & Hankins (1999). However, the authors mainly concentrated on linear polarization. Therefore, we proposed linear and circular polarization observations with a very high time resolution at 1.38 GHz (**H1**). Results from this study are described below.

The observations of the full linear and circular polarization of the Crab pulsar were performed with the Westerbork Synthesis Radio Telescope (WSRT) in the Netherlands at 1.38 GHz. The WSRT observations, on August 8th, 2011 used 14 25 m diameter dishes combined coherently to form the equivalent of a 94 m dish for pulsar observations. Owing to the interferometric nature of the WSRT, the observations partially resolve out the radio-bright Nebula, thus improving sensitivity over typical single-dish observations. Moreover, as the WSRT is an equatorially mounted telescope, there is no need to correct for the parallactic angle.

At a resolution of 1/8192 of the 34 milliseconds pulse period (i.e., 4.1  $\mu$ s), the 1.38 GHz linear polarization measurements are in general agreement with previous lower-time-resolution 1.4 GHz measurements of linear polarization of three components: MP, IP and LFC. We find the MP and IP to be linearly polarized at about 24% and 21% with no discernible difference in polarization position angle. However, contrary to theoretical expectations and measurements in the visible, we find no evidence for significant variation (sweep) in the polarization position angle over the MP, the IP, or the LFC. We discuss the implications, which appear to be in contradiction to theoretical expectations. We also detect weak circular polarization in the MP and IP, and strong ( $\approx$ 20%) circular polarization in the LFC, which also exhibits very strong ( $\approx$ 98%) linear polarization at a position angle of 40° from that of the MP or IP. The properties are consistent with the LFC, which is a low-altitude component, and the MP and IP, which are high-altitude caustic components. Current models for the MP and IP emission do not readily account for the absence of pronounced polarization changes across the pulse. The pulse phase of the IP and LFC measured in reference to the pulse phase of MP are consistent with the previous measurements, that have shown that the phases of these pulse components are evolving with time.

Our analysis of the radio Stokes data shows no strong sweep of the linear-polarization position angle. This lack of strong position-angle swings contrasts with the rapid swings observed in the visible band (Fig. 2). Current models for pulsar emission geometries do not readily account for the absence of substantial variations in both polarization degree and position angle across a pulse component. Thus, alternative models – e.g., dissipative magnetospheres – should be considered in modeling the radio polarization of the Crab pulsar’s MP and IP. The nearly complete polarization of the LFC suggests that it originates at a different location and via a different mechanism than do the stronger MP and IP. Finally, the fine time resolution and high signal-to-noise ratio in the MP data led to the detection of a statistically significant substructure in its pulse profile. We surmise that this substructure results from giant radio pulses occurring during the 144-minute observation.

The most important outcome from the results presented in **H1** is that the characteristics of

---

<sup>1</sup><http://www.mpe.mpg.de/270643/OPTIMA>

<sup>2</sup>Partly the results presented in Słowikowska et al. (2009) were used in my PhD thesis, therefore this publication is not discussed here in details.

the radio linear polarization of the MP and IP resemble neither those of caustics in existing geometric models nor those observed in the optical emission. The lack of position angle swing in the radio MP and IP is in stark contrast to the rapid position-angle swings in the optical. The very low circular polarization and moderate linear polarization observed here in the radio MP and IP are consistent with caustics, but the observed linear-polarization values ( $\approx 22\%$ ) in the radio are significantly higher than those in the optical, and there is only a small variation with phase in the MP. On the other hand, the radio pulses are much narrower than the optical pulses, indicating that the radio MP and IP may originate along a smaller range of altitudes and/or in a subset of field lines.

### 4.3 Optical polarimetry studies of white dwarfs [H2, H3]

There are more than thousands of WDS known up to date, more than 40,000 confirmed WDs in the SDSS catalogue and almost 500,000 WD candidates proposed by the Gentile Fusillo et al. (2019) after Gaia DR2 release. For some of them, the spectral type is known. Most WD atmospheres are hydrogen-rich (DA), and almost all the rest are helium-rich (DB). However, a significant fraction of WDs also contain traces of heavier elements in their atmospheres, and these are labelled with Z for metals or Q for carbon, for example, DZ or DQ. There are also WDs for which the spectrum does not show any strong lines, but their atmospheres are still helium-rich. Such WDs are classified as DC-type WDs.

In the publication **H2** and **H3** we present results of the optical linear polarimetric survey of 101 white dwarfs (WDs) performed with the RoboPOL polarimeter (King et al., 2014). We have isolated DA-, DB- and DC-type od WDs in our sample, as well as the WDs in binary systems. In case of binary systems usually the WD companion is the red dwarf (dM), i.e. DA + dM systems. However, we also have some double degenerated systems (DDSs) and four systems with WD of DB-type, in our sample.

The aim of our work is twofold: (i) to perform a statistical analysis of the linear polarization properties of a WD sample; and (ii) to provide observers with new faint linear polarimetric standard sources. Many polarization studies of large samples of WDs have been conducted to date. The crucial difference between the previous studies and our work is that our observations represent the first WD linear polarization (in continuum) survey, whereas the others measured the circular polarization (in spectral lines). Moreover, the scientific community has started to use polarimetric measurements extensively to study stellar and non-stellar objects. However, attempts to reach fainter objects using infrastructure with larger mirrors have encountered a serious problem, namely a lack of faint polarization standards of both types – zero-polarized and polarized.

The RoboPOL<sup>3</sup> polarimeter is based on two Wollaston prisms and by this gives simultaneously measurements that allow to determine the Stokes I, Q, U or normalised Stokes  $q = Q/I$  and  $u = U/I$ . We performed the polarization observations of a selected sample of WDs through the R filter. Therefore, we measured the polarization of the continuum. Our study shows that highly linear polarized white dwarfs are very rare. The distribution of WDs in the colour-magnitude diagram, as well as the Galaxy is shown in Fig. 3.

We find that the median polarization degree of isolated DA WDs and DB WDs are similar, but lower than the median polarization of isolated DC WDs (Fig. 4, left). The DB WDs in binaries seem to be more polarized than binaries containing DA+dM or double degenerated systems (DDSs) with DA component (Fig. 4, right).

Within our sample, we found three targets with PD higher than 1%. WD1415+234 is an isolated DB WD with PD of 2.66%. This value of the PD does not depend on the chosen aperture. A

---

<sup>3</sup><http://robopol.org/>

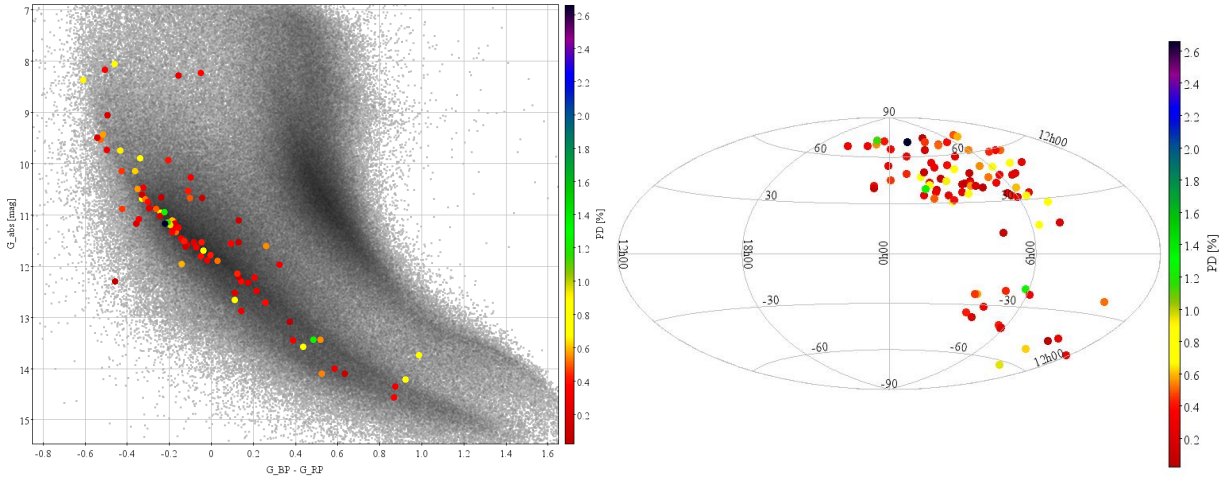


Fig. 3. *Left*: RoboPOL sample of white dwarfs over plotted on the color-magnitude diagram. Grey points represent the WD candidates selected from the second data release of the Gaia DR2 (Gentile Fusillo et al., 2019). The colour bar indicates the PD observed value. *Right*: Galactic distribution of RoboPOL WD sample in the Aitoff projection. The colour bar indicates the PD observed value.

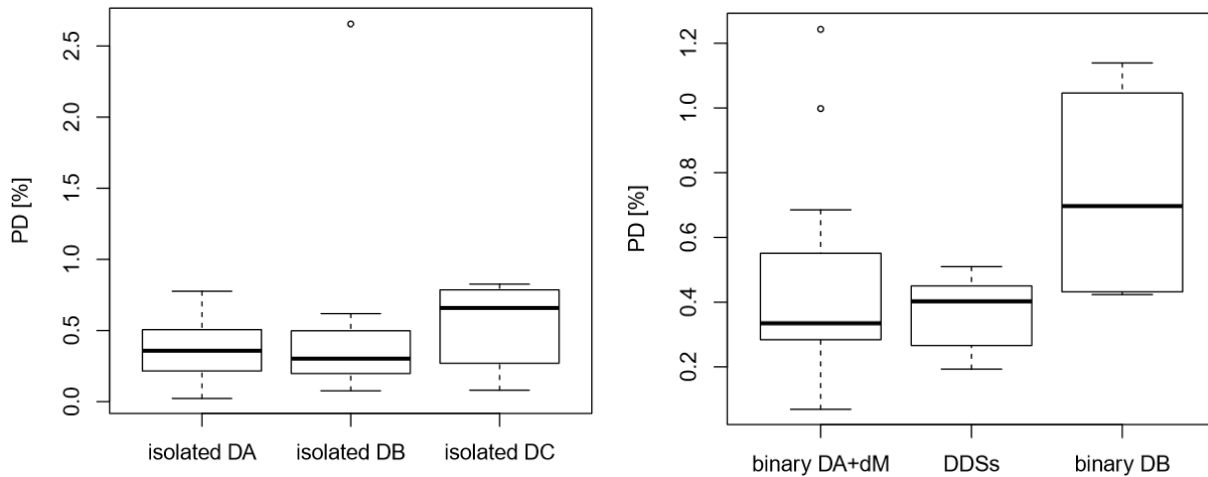


Fig. 4. *Left*: Median PD of three spectral types of isolated WDs, i.e. DA-, DB-, and DC-type in the form of a box plot. There are 63 DA-type WDs, seven DB-type WDs, and six DC-type WDs in our sample. The thick black line inside the rectangle denotes the median value of the sample. The rectangle covers 50 per cent of the points lying between the 1st and 3rd quartiles. The upper and the lower whiskers denote either extremal values from the data set (maximum or minimum, respectively) lying in the 1.5 IQR (interquartile range) distance from the rectangle or 1.5 IQR itself, whichever is closer. The outlier, WD1415+234 with PD~2.6%, lying outside the whisker range is plotted individually as an open circle. *Right*: Comparison of the PD of DA+dM binaries, DDSs and binaries in which one of the components is DB WD is presented as a box plot. Both data sets from 2014 [H3] and 2016 [H2] are used. There are 11 DA+dM binaries, 7 DDSs and 4 with DB-type WDs. There are no DC-type WDs in binary systems other than a component of DDSs in our total sample (DA+DC). The outliers, namely WD1440-025 and WD2213+317, lying outside the whisker range are plotted individually as open circles.

close examination of its neighbourhood stars indicates that the WD polarization is intrinsic. The other two WDs are WD1336+123 and WD1619+123 with the PD values of 1.14% and 1.25%, respectively. Both of them are in binary systems. WD1336+123 is DB spectral type with dwarf M4 companion and WD1619+123 is of DA type with dG0 companion.

- WD1336+123 (PG 1336+124, LP 498-26): we were able to measure its companion (dwarf M4) separated by  $87''$  (Oswalt et al., 1988). It has  $PD = 0.34\% \pm 0.33\%$ , while  $PA = 82^\circ.4 \pm 25^\circ.4$ . This compares with WD  $PD = 1.14\% \pm 0.15\%$  and  $PA = 2^\circ.3 \pm 3^\circ.9$ . The maximum PD caused by the ISM is about 0.42%. Therefore, the measure PD of the WD itself is intrinsic.
- WD1619+123 it is an SLS with a dwarf G0 companion separated by  $63''$  (Farihi et al., 2005). It can be resolved by RoboPOL, but unfortunately, it was covered by the mask even in the pointing exposures. Holberg et al. (2013) give the position angle of the companion, where the orientation is measured from the WD to the companion, being  $311^\circ.39$  (that corresponds to  $131^\circ.39$ ) and it is aligned with the proper motion position angle of  $135^\circ.8$  found by Farihi et al. (2005).

Within our sample, we have two common proper motion binary systems (CPMBs): WD1336+123 and the Sirius-like system (SLS) WD2129+000. In both cases measured PD of the companions (dwarf M4 in case of WD1336+123 and K2 in case of WD2129+000) is smaller than the expected maximum  $PD_{ISM}$ . Such measurements give an independent check on the contribution of the polarization degree from the ISM, assuming that no intrinsic PD is expected from the companions — M4 and K2 type dwarfs. Other binary systems and one multiple system are discussed in details in **H2**.

Highly linear polarized white dwarfs are very rare. Hence, the recent discovery of the first pulsar-like WD (AR Sco, Buckley et al., 2017) has awakened great interest. AR Sco is a close binary with an orbital period of 3.56 hours consisting of a red dwarf of M spectral type and a WD. The WD of AR Sco has a 117 second rotational period and shows very strong linear polarization variations as a function of its spin period. This behaviour is very similar to the polarization changes observed in the Crab pulsar (Słowiowska et al., 2009, 2012).

The main result of the WDs survey ([**H2**] and [**H3**]) is the indication that the isolated DC-type WDs have higher polarization degree measured in continuum than isolated DA-type or DB-type WDs. Additionally, there is an indication that the binary systems with one of the components being a helium-rich WD (i.e. DB-type WD) show higher polarization degree than the DA+dM binaries or DDSs. It might indicate that the isolated DB-type WDs have different characteristics than DB-type WDs in the binary systems.

#### 4.4 What should we worry about while performing polarimetric observations? [**H4**]

The importance of the proper calibration of any polarimeter is described in this section, where calibration of the RINGO3 polarimeter at the Liverpool Telescope is presented. During our very detailed analysis, we found out that for some epochs the proper calibration of the RINGO3 is not possible [**H4**].

The 2.0-m Liverpool Telescope (Steele et al., 2004) is the biggest fully robotic telescope on the world and RINGO3 (Arnold et al., 2012) is a fast-readout optical imaging polarimeter. Unlike the original RINGO<sup>4</sup> which used deviating optics to spread the time-varying polarised signal into rings, RINGO3 uses a fast readout camera to capture this signal as it changes in time. It is fed

---

<sup>4</sup><http://telescope.livjm.ac.uk/TelInst/Inst/RINGO/>

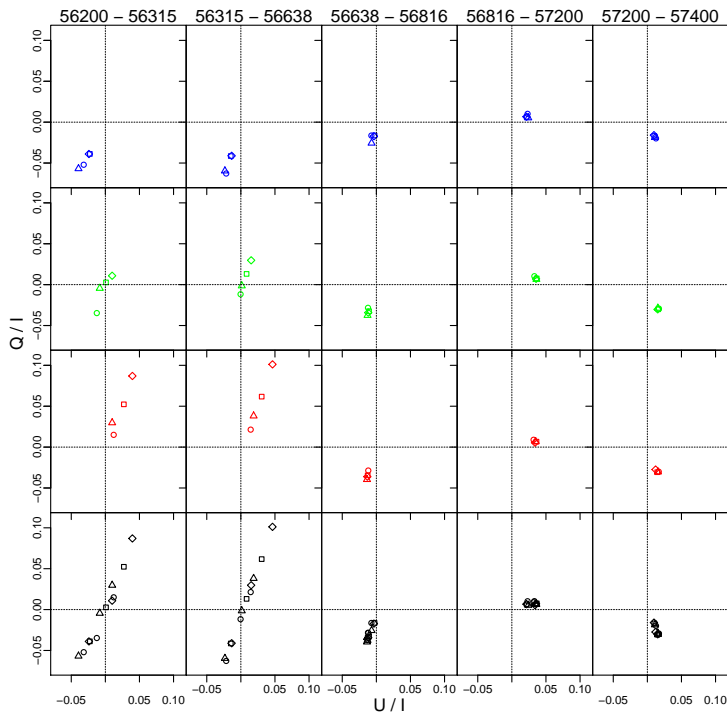


Fig. 5. Weighted means of the normalised Stokes Q/I and U/I parameters for the unpolarised standard stars G 191-B2B (rhombus) and HD 14069 (square) and the centres of fitted circles for polarised standard stars BD +59 389 (circle) and BD +64 106 (triangle) as a function of time (five epochs in MJD). The bottom row contains all the points in all colours for all the standard stars for each epoch. The scatter of points is highest in the first two epochs (56200–56638 MJD) with the lowest value of scattering in the case of the blue camera and the biggest for the red one. In the last two epochs of 56816–57200 MJD and 57200–57400 MJD all the points are gathered around the same point which is very close to zero-zero. It shows that the hardware changes improved the system significantly.

by a 45-degree folding mirror from the telescope main beam. It is this time-varying signal that the instrument records to measure the polarization of light entering the instrument. Following the rotating polariser, a collimator lens is used to collimate the beam. A pair of dichroic mirrors then splits the beam into three for simultaneous polarised imaging in three wavebands with the separate camera lens and detector systems with approximate wavelength ranges of blue 350–640 nm, green 650–760 nm and red 770–1000 nm. The colours of the RINGO3 cameras therefore approximately correspond to the B+V, R and I Johnson filters respectively. Each camera receives eight exposures per polariser rotation. These exposures are electronically synchronised with the phase of the polariser’s rotation. All frames for each matched phase are then stacked to obtain a single image at each phase of the polariser’s rotation for data analysis.

To calculate the Stokes I, Q, and U we used method described by Sparks & Axon (1999) for n-polarisers. This method was very successfully used before. One of the most extreme cases of using the n-polarisers method is the case of the Crab pulsar presented by Słowikowska et al. (2009) where measurements through as many as 180 positions of the rotating polariser were used to calculate PA and PD as a function of the Crab pulsar rotational phase with a time resolution of 4  $\mu$ s. The most significant advantage of using more than three polarisers is the substantial reduction in the errors of PD and PA. For each source, we calculated normalised Stokes parameters  $q=Q/I$  and  $u=U/I$  for data acquired from all three cameras.

The great advantage of the LT is that all observations of standards (photometric, spectroscopic and polarimetric) are public. Therefore, we were able to analyse data of the zero-polarized as well as high polarized standard stars gathered over more than three years (i.e. more than 100,000 frames). Within this period, there were four hardware changes that introduce changes in the polarimeter performance. Therefore, there are five epochs for which we checked the RINGO3 polarimeter characteristics. The most important results of this work are shown in Fig. 5. There is a significant scatter of points in the first two epochs that covers the time span from 56200 MJD to 56638 MJD. However, in the next epochs, the system is getting more stable in terms of instrumental polarization. The centres (of each polarization standard) have similar coordinates for each source which means that they translate to the same instrumental polarization values.

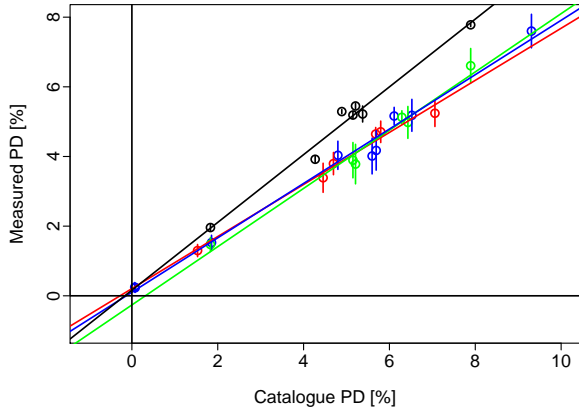


Fig. 6. Measured PD as a function of catalogued PD for the blue, green and red cameras of the RINGO3 polarimeter (colour coded). The colours of the RINGO3 blue, green and red cameras approximately correspond to the B+V, R and I, respectively. For comparison, the RoboPOL polarimeter data are also shown (black points and solid black line, after Table 1 of King et al. (2014)). RoboPOL polarimeter works in the Johnson R-band.

This way one is able to remove the instrumental contribution to the measured PD of the target. The relationship between the RINGO3 values and the catalogue ones are shown in Fig. 6. For comparison the measured values of seven high polarization standards (for details check the Table 1 of King et al., 2014) obtained with the RoboPOL polarimeter are shown.

We show that the data taken with RINGO3 polarimeter have to be taken with caution if they were obtained within the time span 56200 – 56638 MJD (i.e. first two epochs). During that period the proper calibration of the instrument is not possible. Why? Our data analysis shows that during these two epochs the measured polarization degree of the observed source does not depend on its true polarization degree, which of course can not be true. Therefore, one needs to be very careful while interpreting results obtained from RINGO3 polarimeter during these two epochs. Such results can easily be artefacts. Thus their physical interpretation is most likely meaningless.

The present work is useful not only for RINGO3 users but also as a reference for anyone performing polarimetric observations. This data set is an invaluable source of information, while it not only helps to calibrate the RINGO3 polarimeter but also helps to study the stability of polarimetric standard stars, e.g. a white dwarf standard G191-B2B.

Our results have been already used for example in the discussion of the calibration of the RoboPOL (Ramaprakash et al., 2019). Recently, Maund et al. (2019) in the publication entitled *RINGO3 polarimetry of the Type I superluminous SN 2017egm*, followed our prescription to calibrate for the effects of polarization induced by the RINGO3 instrument.

#### 4.5 Optical high time resolution observations of intermediate polar and magnetar [H5, H7]

The next frontier for observational astrophysics will be the temporal domain below 1 second, where the physics and astrophysics of compact objects become essential. Traditionally, optical astronomy has been concerned with timescales measured from minutes and hours to years. Sub-minute and particularly sub-second timing has been mostly unexplored primarily due to instrument/detector limitations. High Time Resolution Astrophysics<sup>5</sup> (HTRA, Shearer et al., 2010) concerns itself with observations on short scales usually defined as being lower than the standard read-out time of a CCD. As such it is concerned with condensed objects such as neutron

<sup>5</sup><https://pos.sissa.it/108/054/>

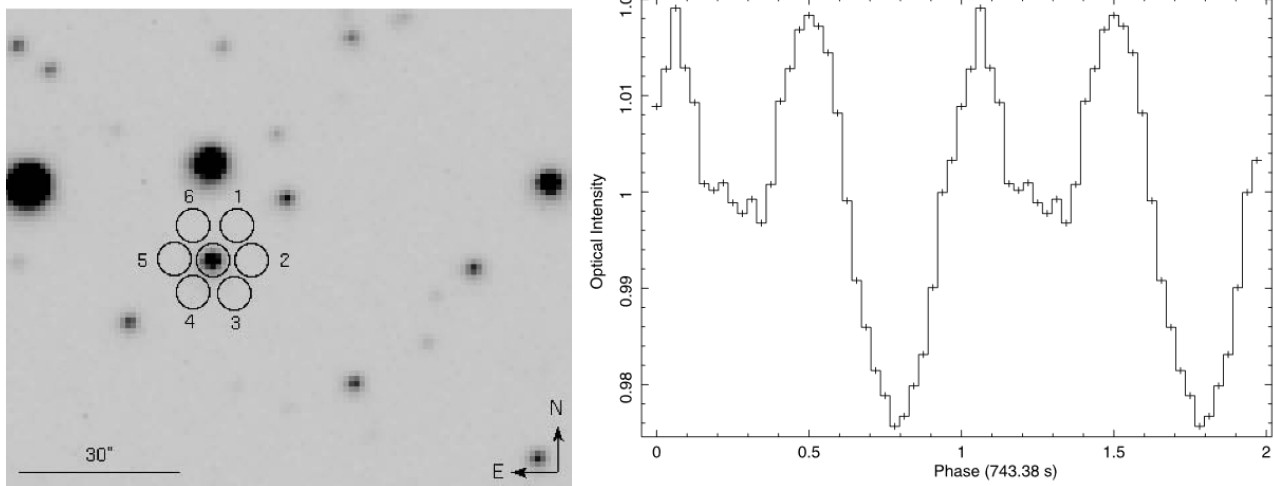


Fig. 7. *Left*: OPTIMA fibre bundle centred on V2069 Cyg. OPTIMA is a fibre-fed system using six fibre apertures in a hexagonal bundle around the target fibre, plus one additional, more distant background fibre to determine and subtract the sky background. All apertures are of  $300\mu\text{s}$  diameter, corresponding to 6 arc seconds on the sky with the SKO 1.3m telescope. The photon-counting mode of OPTIMA has an intrinsic photon-arrival-time resolution of  $4\mu\text{s}$  and records unfiltered white light radiation in the wavelength range 450-900 nm, with peak efficiency around 700 nm. The ring fibres (1–6) are used to monitor the background sky simultaneously. *Right*: Pulse profile obtained from all OPTIMA data folded with the 743.38 s spin cycle (32 bins per period). The profile is background subtracted and normalized to the average count rate of 4621 counts/s.

stars, black holes and white dwarfs, surfaces with extreme magnetic reconnection phenomena, as well as with planetary scale objects through transits and occultations. HTRA is the only way to make a significant step forward in our understanding of several important astrophysical and physical processes; these include the extreme gravity conditions around neutron stars and stable orbits around stellar mass black holes.

Many HTRA instruments are based on the Single Photon Avalanche Diodes (SPADs). Some examples of such detectors are OPTIMA (Kanbach et al., 2003), GASP (Collins et al., 2008, 2013), AquEYE and IquEYE (Barbieri et al., 2009, 2012; Naletto et al., 2009) which can measure the time of arrival of a single optical photon with an accuracy of down to 50 picoseconds. These detectors are successfully used to study rapidly changing sources such as optical pulsars (Słowikowska et al., 2009, 2012; Spolon et al., 2019), cataclysmic variables, including polars and intermediate polars [H5] and very fast flares from optical magnetar [H7]. Recently the first detection of an optical millisecond pulsar PSR J1023+0038 with the fast photon counter Aqueye+ (Zampieri et al., 2019) was reported.

#### 4.5.1 Intermediate polar V2069 Cyg [H5]

I proposed the observation of the intermediate polar V2069 Cyg with the OPTIMA photopolarimeter in 2009. OPTIMA was mounted at the 1.3-m telescope of the Skinakas Observatory<sup>6</sup> (SKO) from 2006 until 2012. Since then it was called OPTIMA-Burst. The main aim of these observing campaigns was to catch the optical afterglows of the Gamma Ray Bursts (GRBs) immediately after the detection by the *Swift* satellite. Along with optical observations of V2069 Cyg with the OPTIMA detector, I asked for the simultaneous observations on board of the *Swift* satellite. We obtained simultaneous optical and X-ray data (*Swift* XRT, 0.3–10 keV), both profiles are shown in Fig. 6 and 7 of Nasiroglu et al. (2012), respectively. 18.7-h observations of V2069 Cyg with the OPTIMA detector allowed us to obtain very detailed double peak light

<sup>6</sup><http://skinakas.physics.uoc.gr/en/>

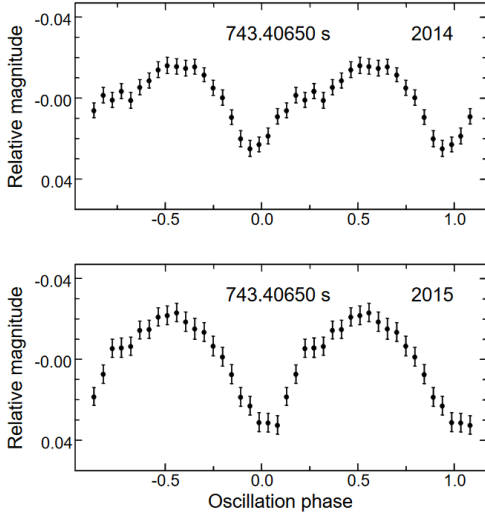


Fig. 8. Pulse profiles with a period of 743.40650 seconds of two oscillations of V2069 Cyg obtained by Kozhevnikov (2017) in 2014 and 2015. It shows an asymmetric shape in 2014, while it changes to a quasi-sinusoidal shape in 2015.

curve of the white dwarf (Fig. 7). The spin period observed in the optical range is  $743.38 \pm 0.25$  s. We also obtained the X-ray light curve of V2069 Cyg from the *XMM-Newton* telescope and the spin period is  $742.35 \pm 0.23$  s in this case. Butters et al. (2011) got the rotation period of the WD of  $743.2 \pm 0.9$  s from the *RXTE* data (2–10 keV). The *Swift* and *RXTE* light curve show similar double-peak structure with the maxima located at the 0.3–0.4 and 0.7–0.8 phase. However, the *Swift* light curve suffer due to much lower statistics. The energy ranges of these light curves are similar, but not the same, and this might also introduce some differences. Light curves in X-ray and optical emissions show partly anti-correlated double-peaked forms. It might indicate different emission regions in a weakly magnetized WD, i.e. X-rays come from the accreting polar caps, and optical emission originates from a larger X-ray heated area on the WD. We investigated the pulse shape of the rotating WD as the function of the orbital phase of the binary system. The orbital period of V2069 Cyg is 7.48 hours. For this purpose, we obtained the WD pulse profiles in four orbital phase ranges: 0.0–0.25, 0.25–0.5, 0.5–0.75 and 0.75–1.0. There is some indication of a profile change, especially in the orbital phase range 0.5–0.75, for both optical (Fig. 7) and X-ray light curves.

Additionally, we performed the X-ray spectral analysis of the V2069 Cyg data from the *XMM-Newton* satellite. The X-ray spectra of V2069 Cyg are described by thermal plasma emission (kT of 20 keV) plus a soft black body component with complex absorption and an additional fluorescent iron K emission line, which originates on the WD surface (at 6.4 keV, with an equivalent width of 243 eV).

The optical very detailed double-peaked light curve obtained from the OPTIMA data is a spectacular result in the context of later work presented by Kozhevnikov (2017). Kozhevnikov observed this system photometrically for almost 120 hours in 2014 and 2015 with the time resolution of 4 seconds. In addition to the intense flickering, the pulse shape of V2069 Cyg reveals changes in its profile. The profile was a double-peaked profile in 2009 (Fig. 7, right), while in 2014 it changed to semi sinusoidal pulse shape with some pronounced humps and turned to be quasi-sinusoidal in 2015 (Fig. 8). Such drastic changes of the optical spin pulse profile seem very interesting and uncommon among other intermediate polars. Therefore, this source is an exciting target for further studies with high time resolution instrumentation, not only photometers but also polarimeters to explain the profile changes.

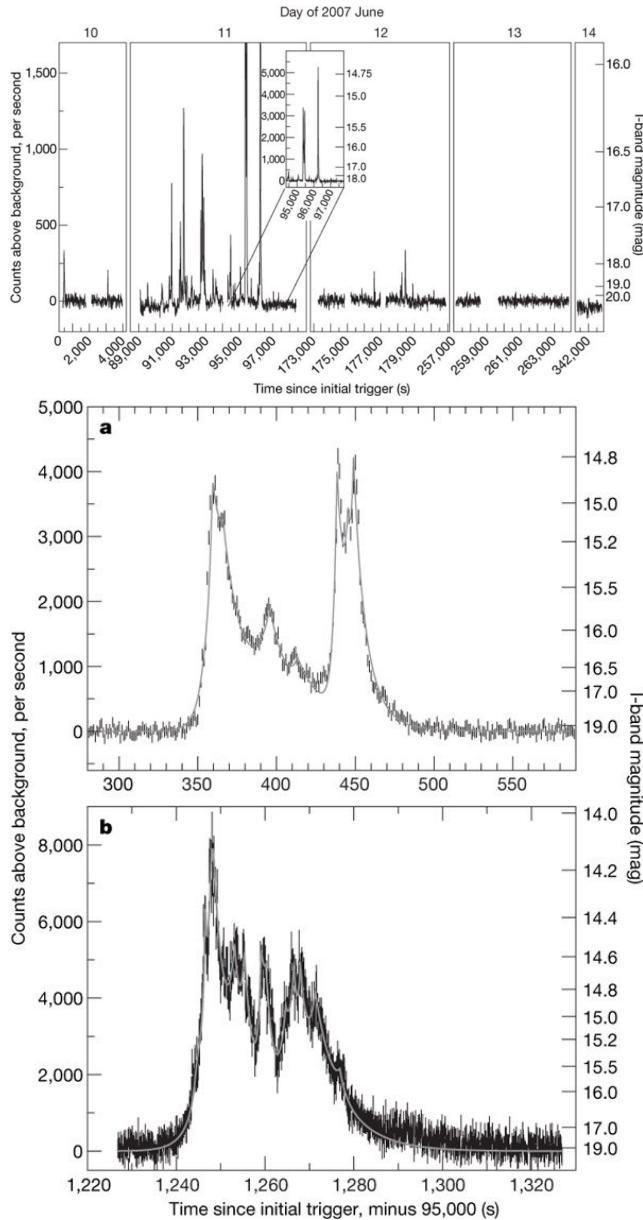


Fig. 9. *Upper panel:* The J1955 light curve recorded by the OPTIMA-Burst detector. The two most prominent flares, at 95,400 s and 96,250 s post trigger, are too bright to be shown adequately next to the rest of the flares and are therefore displayed on a different scale in the inset (middle and lower panels). Simultaneous I-band (630–1010-nm) observations, obtained with the IAC80 telescope of the Instituto de Astrofísica de Canarias (Castro-Tirado et al., 2008), were used to calibrate count rate to magnitudes. *Middle and lower panels:* Zoom in around the two most prominent flares of J1955 as marked in the upper panel. The data in the middle panel are binned with a 1-s resolution, while in the lower panel with a 0.1-s resolution to ensure the reasonable signal-to-noise ratio but also resolve the fastest variabilities detected in the data. The error bars are  $1\sigma$  statistical errors. Extremely fast variability is visible and well resolved. The solid line in each panel is the result of a simple model, consisting of a superposition of several fast-rise, exponential-decay (FRED) subflares.

#### 4.5.2 Optical magnetar [H7]

During the OPTIMA-Burst observing campaigns at the SKO while *hunting* for the possibility to measure the polarization of the optical GRB afterglow we caught another interesting source. In the OPTIMA-Burst mode, the telescope was reacting to the Gamma-ray Coordination Network alerts that provide the distribution of GRBs (and other transients) locations detected by various spacecraft and distributes to the world. After receiving such an alert, the telescope automatically moved to the field and started positioning on the coordinates posted in the GCN alert.

SWIFT J195509.61261406 was discovered as the gamma-ray burst GRB 070610 using the Burst Alert Telescope (BAT) on board the NASA *Swift* spacecraft. Subsequent observations in the X-ray (using *Swift's* X-ray telescope (XRT) and the NASA *Chandra X-ray Observatory*) and the optical bands have shown a point source compatible with the BAT error circle. The optical and X-ray afterglow behaviour indicates that it was caused probably not by a gamma-ray burst, but rather by a Galactic X-ray transient. It was therefore re-assigned the name SWIFT J195509.61261406 (hereafter SWIFT J1955).

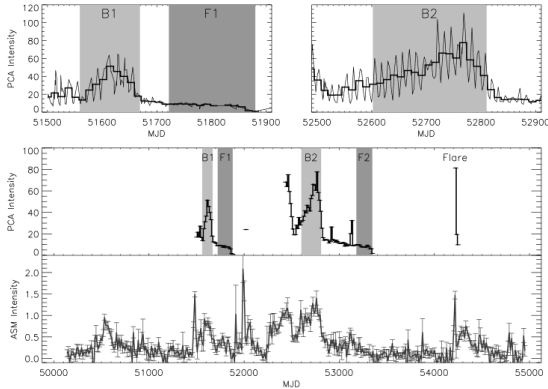


Fig. 10. Bottom panel: RXTE/ASM light curve (1.3-12.1 keV) since 1996 April. A bin size equal to the orbital period,  $P_{\text{orb}}=12.67$  d is used. Middle panel: RXTE/PCU2 (2-60 keV) light curve showing bright (B1, B2) and faint states (F1, F2). Top panel: a detailed view of the PCU2 light curve. The 12.7 d binned PCA light curve is superposed on the average count rate per observation interval (typically, a few thousand seconds integration time). Note the modulation of the X-ray intensity with the orbital period during the bright states and the lack of it during the faint state.

Optical observations with the OPTIMA-Burst detector began just 421 s after the BAT trigger. We gathered 8.5 h of data during the five nights after the burst. The most exciting parts of these data are shown in Fig. 9. We observed two very prominent and brief flares in the optical light curve after the high-energy trigger announced in the GCN alert. The shortest timescales found in our analysis (Fig. 9, middle and lower panel) are 0.3-0.4 s, that corresponds to the region of emission of about  $10^{10}$  cm (i.e. 1/10 of the Solar radius).

At the same time, this source was observed by the group of astronomers led by Castro-Tirado et al. (2008). They detected more than forty flares in the optical band over three days, as well as the IR flare. Optical and near-infrared emission has been observed previously in AXPs and one SGR, but not with flaring variability. Considering the similarities between the optical light curve observed from SWIFT J1955 and X-ray light curves of SGR outbursts, it is conceivable that these are observations of optical flares in a magnetar.

SWIFT J1955 might be a member of a subgroup of soft gamma repeaters (SGRs) for which the long-term X-ray emission is transient. It was the first time when flares in optical and IR bands were detected for the SGR. The extreme variability of SWIFT J1955 in the magnitude and timescales, as well as independent multi-wavelength arguments, suggest the connection to its magnetar nature. This source might be a missing link between the “persistent” SGRs and the dim isolated neutron stars.

#### 4.5.3 SAX J2103.5+4545 the high-mass X-ray binary

SAX J2103.5+4545 is the Be/X-ray binary (BeX) with the shortest orbital period. It shows extended bright and faint X-ray states that last for a few hundred days. We investigate the relationship between the X-ray and optical variability and characterize the spectral and timing properties of the bright and faint states. We find that there is a correlation between the spectral and temporal parameters that fit the energy and power spectra. Softer energy spectra correspond to softer power spectra. It means that when the energy spectrum is soft, the power at high frequencies is suppressed. Additionally, from our  $H\alpha$  line monitoring of the optical counterpart, we find the correlation between the strength and shape of the  $H\alpha$  line, originated in the circumstellar envelope of the massive companion and the X-ray emission from the vicinity of the neutron star.  $H\alpha$  emission, indicative of an equatorial disc around the B-type star, is detected whenever the source is bright in X-rays. When the disc is absent, the X-ray emission decreases significantly.

From our study, we find a good correlation between the strength and profile of the  $H\alpha$  line and the X-ray activity of the source. Emission-line profiles are observed during bright X-ray states. In these states, the equivalent width of  $H\alpha$  is largest. During faint X-ray states,  $H\alpha$  appears in absorption. SAX J2103.5+4545 exhibits the fastest time-scales for the disappearance and

reformation of the circumstellar disc, compared to other typical BeXs. In less than two years, SAX J2103.5+4545 is capable of forming and losing the disc. Due to its narrow orbit, the neutron star prevents the disc from extending to large radii; the disc is truncated at 2–3 stellar radii.

Based on the  $H\alpha$  line profile, we set stringent constraints on the size of the circumstellar disc, and we find that its size can reach the Roche-lobe radius of the system (which it is similar to the periastron distance of the two objects). We have also performed for the first time in a BeX a correlated study of the X-ray spectral and timing properties and found a correlation between the shape of the energy spectrum and that of the power spectrum in the bright state. When the energy spectrum is soft, the power at high frequencies is suppressed. This correlation, together with the existence of hard/high and soft/low states, has been interpreted in the context of emission from the accretion column.

## 4.6 Summary

The set of articles, focused on the investigations of compact objects and presented here as my scientific achievement, illustrates my main scientific activities after the doctorate.

Publication **H1** describes the high-time resolution radio polarimetry studies of the Crab pulsar components at 1.38 GHz. It includes both the linear and circular polarization features. The nearly 100% linear polarization of LFC and high circular polarization suggest that it originates at a different location and via a different mechanism than do much stronger MP and IP. Moreover, there is an absence of substantial variation of PD and PA across MP and IP, and it is in stark contrast to the rapid PA swings in optical. Finally, the fine time resolution and high signal-to-noise ratio in the MP data let to the detection of substructures in its pulse profile resulting from the giant radio pulses.

Publication **H2 and H3** demonstrate the ability to carry out both preliminary studies of continuum linear polarization study of white dwarfs, selected according to specific criteria, and large-scale observation campaigns employing polarimetric observational methods. We found that the isolated DC-type WDs have higher polarization degree measured in continuum than isolated DA-type or DB-type WDs. Additionally, there is an indication that the binary systems with one of the components being a helium-rich WD (i.e. DB-type WD) show higher polarization degree than the DA+dM binaries or DDSs. It might indicate that the isolated DB-type WDs have different characteristics than DB-type WDs in the binary systems. We also delivered a catalogue of faint (13-17 mag) zero-polarized standard stars.

Publication **H4** is an example of a report on in-depth investigations of the dedicated instrument for the largest fully robotic telescope on the world, i.e. Liverpool Telescope. We describe the long term performance of the polarimeter RINGO3, and we give the prescription how to calibrate the data obtained with this instrument. Unfortunately, for some time due to the hardware issues, the RINGO3 polarimeter was not performing correctly. Presented calibration is useful not only for RINGO3 users but also as a reference for anyone performing polarimetric observations. This data set is an invaluable source of information to study the stability of polarimetric standard stars. This work is also a case where my previous experience with OPTIMA photopolarimeter was fully used.

Publication **H5** is an example of a reaction to the Astronomers Telegrams, whereas publication **H7** is a reaction to the GCN alerts. Both publications show excellent capabilities of photon counting instrument as the OPTIMA-Burst that allowed us to obtain the very detailed (so far the best) light curve of intermediate polar V2069 Cyg, as well as to discover the first optical magnetar (AXP or SGR) type object. In **H5** we establish the optical and X-ray profiles of V2069 Cyg and we checked their dependence from the orbital phase. We also modelled the X-ray spectrum of V2069 Cyg. The hard X-ray spectrum with an iron line at 6.4 keV is typical of

IPs. **H7** describes very fast optical flaring from a possible new Galactic magnetar. The extreme variability of SWIFT J1955 in the magnitude and timescales, as well as independent multi-wavelength arguments, suggest the connection to its magnetar nature. This source might be a missing link between the “persistent” SGRs and the dim isolated neutron stars. It was the first time when flares in optical and IR bands were detected for the SGR.

Publication **H6** shows my capabilities of working with X-ray data as well on the example of the high mass X-ray binary SAX J2103.5+4545. We showed a correlation between the strength and shape of the  $H\alpha$  line that originates in the circumstellar envelope of the massive companion and the X-ray emission from the vicinity of the neutron star.  $H\alpha$  emission is detected whenever the source is bright in X-rays. During faint X-ray states, when the disc is absent  $H\alpha$  appears in absorption and X-ray emission decreases significantly.

Since my M.Sc. thesis, I have been working on the multiwavelength approach to study compact objects, especially neutron stars and white dwarfs, isolated and in binary systems. I am using various techniques, including polarimetry and HTRA detectors, in radio and optical range of electromagnetic spectrum. Photometry and spectroscopy are well-known and widely used techniques, polarimetry is still not so spread among optical astronomers. However, in recent years there has been a dynamic development of this field of astronomy, and not only in the optical range of the electromagnetic spectrum but also in X-rays.

## 5 Discussion of other scientific achievements.

---

In this discussion I skip my minor contributions to the research activities where my contribution was less than 10%.

### 5.1 Further studies of pulsars

Polarization measurements of pulsars and their synchrotron nebulae offer unique insights into their highly magnetized relativistic environments and a prime test of neutron star magnetosphere and emission models. We address the importance of optical polarization measurements in testing neutron star magnetosphere models. I took part in the following publications referring to such studies (after PhD):

- Mignani, R. P.; Moran, P.; Shearer, A.; Testa, V.; **Słowikowska, A.**; Rudak, B.; Krzeszowski, K.; Kanbach, G., “VLT polarimetry observations of the middle-aged pulsar PSR B0656+14”, 2015, *Astronomy and Astrophysics*, Volume 583, id.A105, 5 pp.,
- Krzeszowski, K.; Maron, O.; **Słowikowska, A.**; Dyks, J.; Jessner, A., “Analysis of single pulse radio flux measurements of PSR B1133+16 at 4.85 and 8.35 GHz”, 2014, *Monthly Notices of the Royal Astronomical Society*, Volume 440, Issue 1, p.457-464,
- Moran, P.; Shearer, A.; Mignani, R. P.; **Słowikowska, A.**; De Luca, A.; Gouiffès, C.; Laurent, P., “Optical polarimetry of the inner Crab nebula and pulsar”, 2013, *Monthly Notices of the Royal Astronomical Society*, Volume 433, Issue 3, p.2564-2575,
- Mignani, R. P.; De Luca, A.; Hummel, W.; Zajczyk, A.; Rudak, B.; Kanbach, G.; **Słowikowska, A.**, “The near-infrared detection of PSR B0540-69 and its nebula”, 2012, *Astronomy and Astrophysics*, Volume 544, id.A100, 9 pp.,
- Mignani, R. P.; Sartori, A.; de Luca, A.; Rudak, B.; **Słowikowska, A.**; Kanbach, G.; Caraveo, P. A., “HST/WFPC2 observations of the LMC pulsar PSR B0540-69”, 2010, *Astronomy and Astrophysics*, Volume 515, id.A110, 11 pp.,

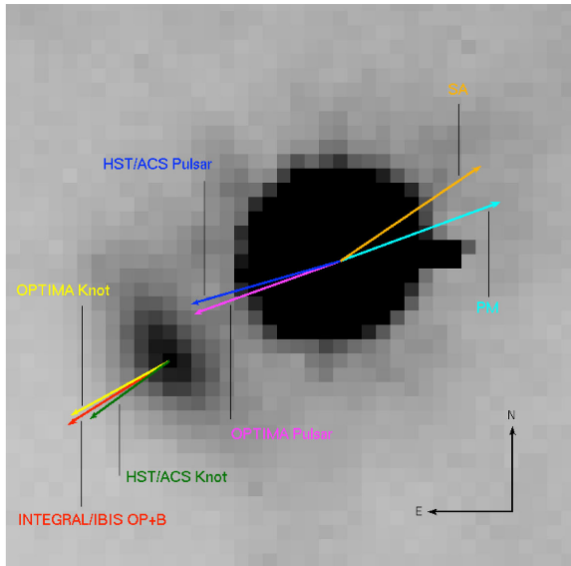


Fig. 11. The Crab pulsar as observed by the HST/ACS camera, FoV  $2'' \times 2''$ . The colour vectors indicate the direction of the position angle measured with the use of different instruments (HST, INTEGRAL, OPTIMA) for given components of the Crab pulsar, i.e. pulsar itself as well as its inner knot (located  $0''.65$  from the pulsar). The proper motion (PM) vector and the spin-axis (SA) vector are plotted as well, for details and references see Fig. 9 of Moran et al. (2013).

- Mignani, R. P.; Bagnulo, S.; Dyks, J.; Lo Curto, G.; Słowikowska, A., "The optical polarisation of the Vela pulsar revisited", 2007, *Astronomy and Astrophysics*, Volume 467, Issue 3, June I 2007, pp.1157-1162.

Polarimetric measurements provide observational constraints on the different models proposed for the pulsar emission mechanisms. Optical polarization data of the Crab nebula were obtained from the Hubble Space Telescope (HST) archive (Moran et al., 2013). The data set consists of a series of observations of the nebula taken with the HST/Advanced Camera for Surveys (ACS). We produced polarization vector maps of the inner nebula and measured, for the first time, the degree of linear polarization (PD) and the position angle (PA) of the pulsar's integrated pulse beam, and its nearby synchrotron knot. It yielded  $PD = 5.2\% \pm 0.3\%$  and  $PA = 105^\circ.1 \pm 1^\circ.6$  for the pulsar, and  $PD = 59.0\% \pm 1.9\%$  and  $PA = 124^\circ.7 \pm 1^\circ.0$  for the synchrotron knot. It is the first high-spatial-resolution multi-epoch study of the polarization of the inner nebula and pulsar. None of the main features in the nebula shows evidence of significant polarization evolution in the period covered by these observations. The results for the pulsar are consistent with those obtained by me (Słowikowska et al., 2009, 2012) using the high-time resolution photo-polarimeter – Optical Pulsar Timing Analyzer (OPTIMA), once the constant component (DC) has been subtracted. Our results prove that the knot is the main source of the DC component. The HST and the OPTIMA results are shown in Fig. 11 and 12, respectively. OPTIMA does not have a spatial resolution, or in other words, its single *pixel* size on the sky is rather big (e.g.  $2''.35$  for the NOT, and  $6''$  for the SKO). However, in case of the pulsar observations and having the exact time of arrival of a single photon, we can perform decomposition for the sky and nebula, pulsar, and the DC component based on the Stokes parameters. Moreover, we can bin the data according to our needs, including the case when only one bin is used and then calculate the phase-averaged polarization degree and position angle for a given data case.

With our VLT measurement (Mignani et al., 2015), linear polarisation values have now been obtained for the brightest pulsars identified in the optical. These data suggest that the pulsar phase-averaged polarisation is lower in the optical than in radio. It might be ascribed to the difference between incoherent and coherent radiation emission mechanisms in the optical and in radio, respectively. We investigate the possible correlation between the phase-averaged optical PD and some physical parameters of studied pulsars such as spin period, spin derivative, characteristic age, the spin down-power, magnetic field at the surface and the light cylinder (Fig. 2 of Mignani et al., 2015). Phase-averaged PD as a function of the characteristic age of pulsars is shown in Fig. 13.

The PD tends to be higher in older and less energetic pulsars, and with the lower value of the magnetic field at the light cylinder. The relatively lower values of PD for younger and more ener-

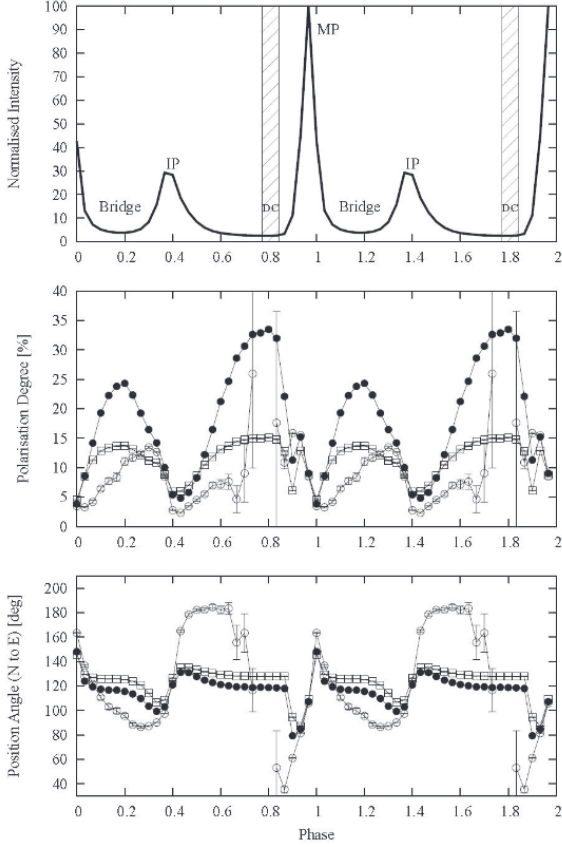


Fig. 12. OPTIMA measurements of the Crab pulsar and inner region of its nebula. Top panel: the Crab pulsar light curve obtained from photons recorded by the OPTIMA central single-photon avalanche diode (SPAD) and after subtraction of the nebular and sky background contribution. The components of the light curve are indicated as follows: MP; IP; non-zero intensity level between MP and IP, i.e. bridge as well as the DC region, previously known as the 'off-pulse' component in the phase range 0.78 - 0.84 being on the level of  $\sim 2\%$  of the MP. Two rotation periods are shown for clarity. Middle and bottom panels show the polarisation degree and position angle (N to E) as a function of pulsar rotational phase, respectively. Data binning is 30 bins per cycle corresponding to 1.12 ms per bin. Three cases are shown: 1) all source of emission are taken into account, i.e. nebula, pulsar and the DC component - it is marked with the open squares; 2) the nebula contribution was subtracted by averaging the Stokes parameters in the hexagonal ring fibres - it is marked with black filled circles; 3) assuming the constant PD and PA component during the DC phase we subtracted corresponding Stokes parameters to obtain pure pulsar polarisation characteristics as its rotational phase. It is plotted with the open circle symbols. Cases 1-3 shows the influence of separated components to the polarisation characteristics, also in the case if one calculates the phase-averaged PD and PA.

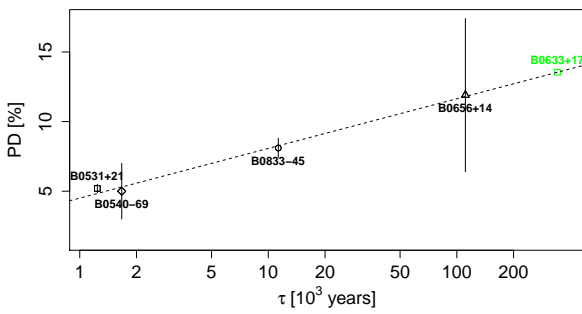


Fig. 13. Measured phase averaged PD of four pulsars: Crab (B0531+21), B0540-69 (pulsar in Large Magellanic Cloud), Vela (B0833-45) and B0656+14 as a function of characteristic age ( $\tau = P(2\dot{P})^{-1}$ ). The dashed line is a linear fit to these four values, while the value for Geminga (B0633+17, marked with green colour) is a fit predicted PD (Mignani et al., 2015).

getic pulsars might be due to the optical emission coming from spatially extended regions of the magnetosphere.

More optical polarisation measurements, covering more extensive ranges in the parameter space, together with the confirmation of the uncertain measurements, will assess the reality of the observed trends and link them to the pulsar physical properties.

## 5.2 Circumbinary planets

The number of discovered extrasolar planets around binary systems is rapidly increasing. These findings have raised the interest in this topic among scientists and consequently drive the development of new detection techniques. Research on circumbinary planets (CBP) has brought us closer to answering fundamental questions about how such planets form and evolve. CBPs properties are probably different from planets found around isolated stars. Many CBPs are found around systems where one of the components is a white dwarf. We are looking for the CBPs by their eclipses timing, and the so-called O-C (observations - calculations) method applied when discussing periodic phenomena. We studied the HU Aqr (Goździewski et al., 2012, 2015) and NSVS 14256825 (Nasiroglu et al., 2017). In the case of the HU Aqr system some of the observations were performed with the use of the OPTIMA instrument, while its egress lasts only 1-2 seconds, see e.g. Fig. 14 (also Fig. 1 of Goździewski et al., 2015). I contributed to the following three publications referring to the CBPs studies:

- Nasiroglu, Ilham; Goździewski, Krzysztof; **Słowikowska, Aga**; Krzeszowski, Krzysztof; Żejmo, Michał; Zola, Staszek; Er, Huseyin; Ogłóza, Waldemar; Drózdź, Marek; Koziel-Wierzbowska, Dorota; Debski, Bartłomiej; Karaman, Nazli, "Is There a Circumbinary Planet around NSVS 14256825?", 2017, *The Astronomical Journal*, Volume 153, Issue 3, article id. 137, 11 pp.,
- Goździewski, K.; **Słowikowska, A.**; Dimitrov, D.; Krzeszowski, K.; Żejmo, M.; Kanbach, G.; Burwitz, V.; Rau, A.; Irawati, P.; Richichi, A.; Gawroński, M.; Nowak, G.; Nasiroglu, I.; Kubicki, D., "The HU Aqr planetary system hypothesis revisited", 2015, *Monthly Notices of the Royal Astronomical Society*, Volume 448, Issue 2, p.1118-1136,
- Goździewski, Krzysztof; Nasiroglu, Ilham; **Słowikowska, Aga**; Beuermann, Klaus; Kanbach, Gottfried; Gauza, Bartosz; Maciejewski, Andrzej J.; Schwarz, Robert; Schwöpe, Axel D.; Hinse, Tobias C.; Haghhighipour, Nader; Burwitz, Vadim; Słonina, Mariusz; Rau, Arne, "On the HU Aquarii planetary system hypothesis", 2012, *Monthly Notices of the Royal Astronomical Society*, Volume 425, Issue 2, pp. 930-949.

HU Aqr is one of the brightest polars discovered so far and consists of a highly magnetized white dwarf and a main-sequence red dwarf. Its O-C residuals were previously attributed to a single  $\sim 7$  Jupiter mass companion in  $\sim 5$  AU orbit or a stable two-planet system with an unconstrained outermost orbit (Goździewski et al., 2012). After three years, we presented 22 new observations of mid-egress eclipse times (Goździewski et al., 2015). Thus, together with already published data, the data set spanned more than twenty years, i.e. from 1993 to 2014. We re-analyse the whole collection of the timing data available. A putative HU Aqr planetary system may be more complex, e.g. highly non-coplanar. Indeed, we found examples of three-planet configurations with the middle planet in a retrograde orbit, which are stable for at least 1 Gyr, and consistent with the observations. The O-C may also be driven by oscillations of the gravitational quadrupole moment of the secondary, as predicted by Lanza-Rodonó effect modification of the Applegate mechanism.

The cyclic behaviour of O-C residuals of eclipse timings in the sdOB+dM eclipsing binary NSVS 14256825 was previously attributed to one or two Jovian-type CBPs. In Nasiroglu et al. (2017) we reported 83 new eclipse timings. These data not only fill in the gaps in the already published time series but also extend the O-C diagram by three years. The O-C diagram revealed a systematic, quasi-sinusoidal variation deviating from a linear ephemeris by about 100 seconds. These variations

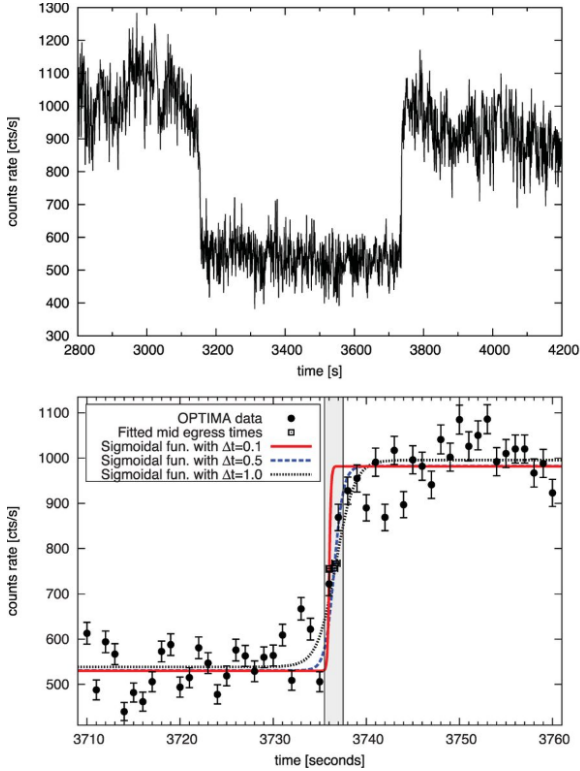


Fig. 14. High time-resolved OPTIMA light curves of HU Aqr. Upper panel: photometric eclipse in the white light. Bottom panel: a close-up around the mid-egress overplotted with three fitted sigmoid functions with different values set for the  $\Delta t$  parameter (0.1, 0.5, 1.0, respectively). Open squares denote the fitted mid-egress times. The shaded region corresponds to a time-span of 2 seconds.

can be caused by either the light propagation time due to the presence of an invisible companion in a distant circumbinary orbit or magnetic cycles reshaping one of the binary components, known as the Applegate or Lanza-Rodonó effect. We found that the latter mechanism is unlikely due to the insufficient energy budget of the M-dwarf secondary. In accordance with the third-body hypothesis, the observed O-C variations in the NSVS 14256825 might be explained by the presence of a single companion with a minimal mass in the brown dwarf mass range (14.7 Jupiter masses), in a moderately eccentric orbit with eccentricity of  $\sim 0.175$ , and the orbital period of  $\sim 10$  years. Our analysis rules out the two-planet model proposed earlier.

Further systematic, long-term monitoring of both systems are required to interpret the O-C residuals and to verify models proposed by us. Additionally, the expected Gaia DR3 data should shed more light on these plausible CBPs by astrometric monitoring of these binaries.

### 5.3 RoboPOL calibration

The RoboPOL calibration is still an ongoing project. Correct calibration of the polarimeter is a critical issue for reliable results of polarimetric measurements. It is achieved by long-term monitoring of highly polarized and zero polarized standard stars to determine instrumental polarization (or depolarization) and the zero-point of the position angle to the North direction. Calibration is also a necessary step to compare measurements from different instruments or the same instrument in a different era.

I am contributing to the RoboPOL collaboration with my experience of calibration of various polarimeters, as well as with my experience as a regular user of the RoboPOL polarimeter. Each instrument requires continuous calibration to ensure proper data analysis and interpretation of the obtained results. While with time we get a better knowledge of the instrument characteristics, therefore, we can also provide better data calibration pipelines. I contributed to the following publication regarding the RoboPOL calibration:

- Ramaprakash, A. N.; Rajarshi, C. V.; Das, H. K.; Khodade, P.; Modi, D.; Panopoulou, G.; Maharana, S.; Blinov, D.; Angelakis, E.; Casadio, C.; Fuhrmann, L.; Hovatta, T.; Kiehlmann, S.; King, O. G.; Kylafis, N.; Kougentakis, A.; Kus, A.; Mahabal, A.; Marecki, A.; Myserlis,

I.; Paterakis, G.; Paleologou, E.; Liodakis, I.; Papadakis, I.; Papamastorakis, I.; Pavlidou, V.; Pazderski, E.; Pearson, T. J.; Readhead, A. C. S.; Reig, P.; **Słowikowska, A.**; Tassis, K.; Zensus, J. A., "RoboPOL: a four-channel optical imaging polarimeter", 2019, Monthly Notices of the Royal Astronomical Society, Volume 485, Issue 2, p.2355-2366.

## 5.4 CTA

I am involved in the Cherenkov Telescope Array (CTA<sup>7</sup>) project by being a member of the Cherenkov Telescope Array Consortium (CTAC). I am working in the Physics group on the multiwavelength observations and study of the TeV sources. I am a member of the group that will support CTA with the optical polarimetric observations and data analysis of the optical counterparts of the TeV sources. From our site, we are going to support the CTA observations by performing the multiband photometric observations at the local observatory of the Toruń Centre for Astronomy (TCfA, Piwnice, Poland) by using 0.9-m Schmidt-Cassegrain telescope (TSC90).

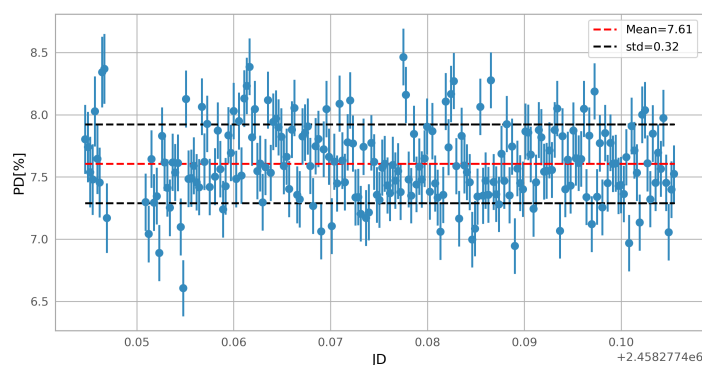


Fig. 15. PD preliminary results of VI-Cyg#12 standard star ( $V=12.54$  mag) obtained with 90cm Schmidt-Cassegrain Telescope at the Toruń Centre for Astronomy. Observations were performed by the consecutive 10 seconds exposures taken through two Savart plates oriented by 45 degrees in respect to each other. Presented results ( $PD=7.61\% \pm 0.32\%$ ) are preliminary without any instrumental calibration and colour filter. The observations are broad band. The literature PD in V is  $8.947\% \pm 0.088\%$  and in R is  $7.893\% \pm 0.037\%$  (Schmidt et al., 1992).

Recently, I have started the polarimetric observations with TSC90 at TCfA. TSC90 is the biggest optical telescope in Poland, and it is equipped with a low-resolution spectrograph, high-resolution Echelle spectrograph and a CCD camera. We added two Savart plates into the rotating filter wheel in 2018. The Savart plates are oriented by 45 degrees in respect to each other, therefore by acquiring consecutive images through the two Savarts, the Stokes Q and U parameters can be reconstructed. First and very preliminary (without any calibration) results of more than a hundred minutes of observations of VICyg#12 with the TSC90 are presented in Fig.15. The results obtained for VICyg#12 star are very promising. The obtained polarization degree on the level of  $7.61\% \pm 0.32\%$  is the evidence that the instrument is working properly and has low induced polarization. TSC90 polarimeter will be calibrated this summer within the framework of one of the Toruń Astrophysics/Physics Summer Program (TAPS) 2019<sup>8</sup> projects.

Moreover, I am a co-investigator in the ESA project "Prototype polarimeter for Near Earth Objects (NEOs)" to build the prototype polarimeter for NEOs. It is foreseen that this polarimeter can be used in the future also for other astrophysical targets, including CTA sources.

## Literatura

- 
- Arnold D. M., Steele I. A., Bates S. D., Mottram C. J., Smith R. J., 2012, in Society of Photo-Optical Instrumentation Engineers (SPIE) Conference Series. p. 2, doi:10.1117/12.927000  
 Barbieri C., et al., 2009, in Photon Counting Applications, Quantum Optics, and Quantum Information Transfer and Processing II. p. 73550Q, doi:10.1117/12.821626

<sup>7</sup><https://www.cta-observatory.org/>

<sup>8</sup>[http://www.home.umk.pl/~astro\\_conf/taps/taps2019/](http://www.home.umk.pl/~astro_conf/taps/taps2019/)

- Barbieri C., Naletto G., Zampieri L., Verroi E., Gradari S., Collins S., Shearer A., 2012, in Griffin E., Hanisch R., Seaman R., eds, IAU Symposium Vol. 285, New Horizons in Time Domain Astronomy. pp 280–282, doi:10.1017/S1743921312000786
- Buckley D. A. H., Meintjes P. J., Potter S. B., Marsh T. R., Gänsicke B. T., 2017, *Nature Astronomy*, 1, 0029
- Butters O. W., Norton A. J., Mukai K., Tomsick J. A., 2011, *A&A*, 526, A77
- Castro-Tirado A. J., et al., 2008, *Nature*, 455, 506
- Collins P., Redfern R. M., Sheehan B., 2008, in Phelan D., Ryan O., Shearer A., eds, American Institute of Physics Conference Series Vol. 984, High Time Resolution Astrophysics: The Universe at Sub-Second Timescales. pp 241–246, doi:10.1063/1.2896936
- Collins P., Kyne G., Lara D., Redfern M., Shearer A., Sheehan B., 2013, *Experimental Astronomy*, 36, 479
- Farihi J., Becklin E. E., Zuckerman B., 2005, *ApJS*, 161, 394
- Gentile Fusillo N. P., et al., 2019, *MNRAS*, 482, 4570
- Goździewski K., Nasiroglu I., Słowikowska A., et al., 2012, *MNRAS*, 425, 930
- Goździewski K., Słowikowska A., Dimitrov D., et al., 2015, *MNRAS*, 448, 1118
- Holberg J. B., Oswalt T. D., Sion E. M., Barstow M. A., Burleigh M. R., 2013, *MNRAS*, 435, 2077
- Kanbach G., Kellner S., Schrey F. Z., Steinle H., Straubmeier C., Spruit H. C., 2003, in Iye M., Moorwood A. F. M., eds, Proc. SPIE Vol. 4841, Instrument Design and Performance for Optical/Infrared Ground-based Telescopes. pp 82–93, doi:10.1117/12.460323
- King O. G., et al., 2014, *MNRAS*, 442, 1706
- Kozhevnikov V. P., 2017, *Ap&SS*, 362, 144
- Manchester R. N., Hobbs G. B., Teoh A., Hobbs M., 2005, *VizieR Online Data Catalog*, 7245
- Maund J. R., Steele I., Jermak H., Wheeler J. C., Wiersema K., 2019, *MNRAS*, 482, 4057
- Mignani R. P., Moran P., Shearer A., Testa V., Słowikowska A., Rudak B., Krzeszowski K., Kanbach G., 2015, *A&A*, 583, A105
- Moffett D. A., Hankins T. H., 1999, *ApJ*, 522, 1046
- Moran P., Shearer A., Mignani R. P., Słowikowska A., De Luca A., Gouiffès C., Laurent P., 2013, *MNRAS*, 433, 2564
- Naletto G., et al., 2009, *A&A*, 508, 531
- Nasiroglu I., Słowikowska A., Kanbach G., Haberl F., 2012, *MNRAS*, 420, 3350
- Nasiroglu I., Goździewski K., Słowikowska A., et al., 2017, *AJ*, 153, 137
- Oswalt T. D., Hintzen P. M., Luyten W. J., 1988, *ApJS*, 66, 391
- Ramaprakash A. N., et al., 2019, *MNRAS*, 485, 2355
- Reig P., Słowikowska A., Zezas A., Blay P., 2010, *MNRAS*, 401, 55
- Schmidt G. D., Elston R., Lupie O. L., 1992, *AJ*, 104, 1563
- Shearer A., Kanbach G., Słowikowska A., et al. 2010, in Proceedings of High Time Resolution Astrophysics - The Era of Extremely Large Telescopes (HTRA-IV). May 5 - 7, 2010. Agios Nikolaos, Crete Greece. p. 54 ([arXiv:1008.0605](https://arxiv.org/abs/1008.0605))
- Słowikowska A., Kanbach G., Kramer M., Stefanescu A., 2009, *MNRAS*, 397, 103
- Słowikowska A., Mignani R., Kanbach G., Krzeszowski K., 2012, in Lewandowski W., Maron O., Kijak J., eds, Astronomical Society of the Pacific Conference Series Vol. 466, Electromagnetic Radiation from Pulsars and Magnetars. p. 37
- Słowikowska A., Stappers B. W., Harding A. K., O'Dell S. L., Elsner R. F., van der Horst A. J., Weisskopf M. C., 2015, *ApJ*, 799, 70
- Słowikowska A., Krzeszowski K., Żejmo M., Reig P., Steele I., 2016, *MNRAS*, 458, 759
- Słowikowska A., Krzeszowski K., Żejmo M., Blinov D., Reig P., 2018, *MNRAS*, 479, 5312
- Smith F. G., Jones D. H. P., Dick J. S. B., Pike C. D., 1988, *MNRAS*, 233, 305
- Sparks W. B., Axon D. J., 1999, *PASP*, 111, 1298
- Spolon A., Zampieri L., Burtovoi A., Naletto G., Barbieri C., Barbieri M., Patruno A., Verroi E., 2019, *MNRAS*, 482, 175

Steele I. A., Smith R. J., Rees P. C., et al., 2004, in Oschmann Jr. J. M., ed., Society of Photo-Optical Instrumentation Engineers (SPIE) Conference Series Vol. 5489, Ground-based Telescopes. pp 679–692, doi:10.1117/12.551456

Stefanescu A., Kanbach G., Słowikowska A., Greiner J., McBreen S., Sala G., 2008, Nature, 455, 503  
Zampieri L., Burtovoi A., Fiori M., Naletto G., Spolon A., Barbieri C., Papitto A., Ambrosino F., 2019, MNRAS, 485, L109

Żejmo M., Słowikowska A., Krzeszowski K., Reig P., Blinov D., 2017, MNRAS, 464, 1294

Toruń, date 26.09.2019

Agnieszka Słowikowska